Supporting Information for:

Dynamics of Polymerization and Gelation in Epoxy Nanocomposites via X-ray Photon Correlation Spectroscopy

Edward B. Trigg[1,2], Lutz Wiegart[3], Andrei Fluerasu[3], and Hilmar Koerner[1].*

1. Materials & Manufacturing Directorate, Air Force Research Laboratory, WPAFB, OH, 45433, United States.

2. UES, Inc. Dayton, Ohio 45432, United States.

3. National Synchrotron Light Source II, Brookhaven National Laboratory, 744 Brookhaven Avenue, Upton, New York 11973, United States.

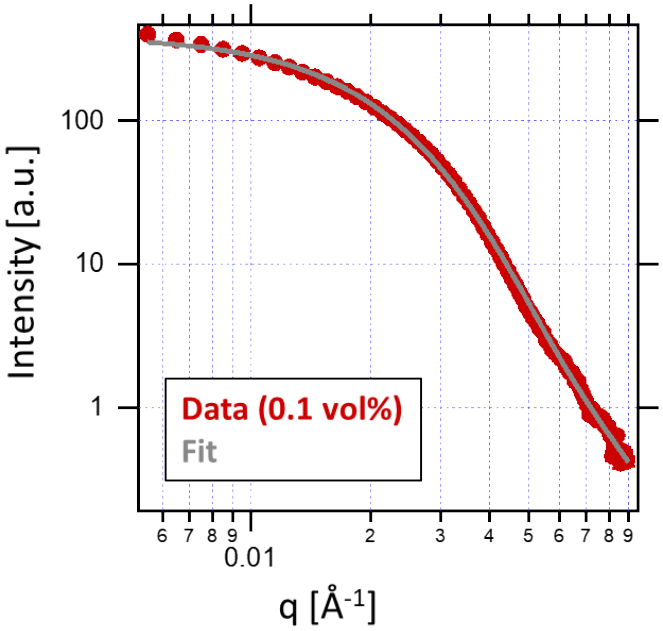

Figure S1. Small-angle X-ray scattering (SAXS) of the dilute NPs (0.1 vol%) in EPON826. The data is shown in red. The data was fit with a polydisperse sphere form factor, where the radii were distributed according to a log-normal distribution. The fit, shown in gray, indicated a volume-average particle diameter of 15.5 nm +/- 5.7.

The SAXS data in Figure S1 was collected on a Xeuss 3.0 (Xenocs) with an X-ray wavelength of 1.542 $Å^{-1}$ and a sample-to-detector distance of 1825 mm. A sample of EPON826 was prepared containing 0.1 vol% loading of NPs. SAXS was collected, and the background (pure EPON826) was subtracted. Samples were loaded into 1.5-mm borosilicate glass capillaries (Charles Supper). The exposure time was 10 hours. The data was fit using Igor Pro with the Irena package.[1]

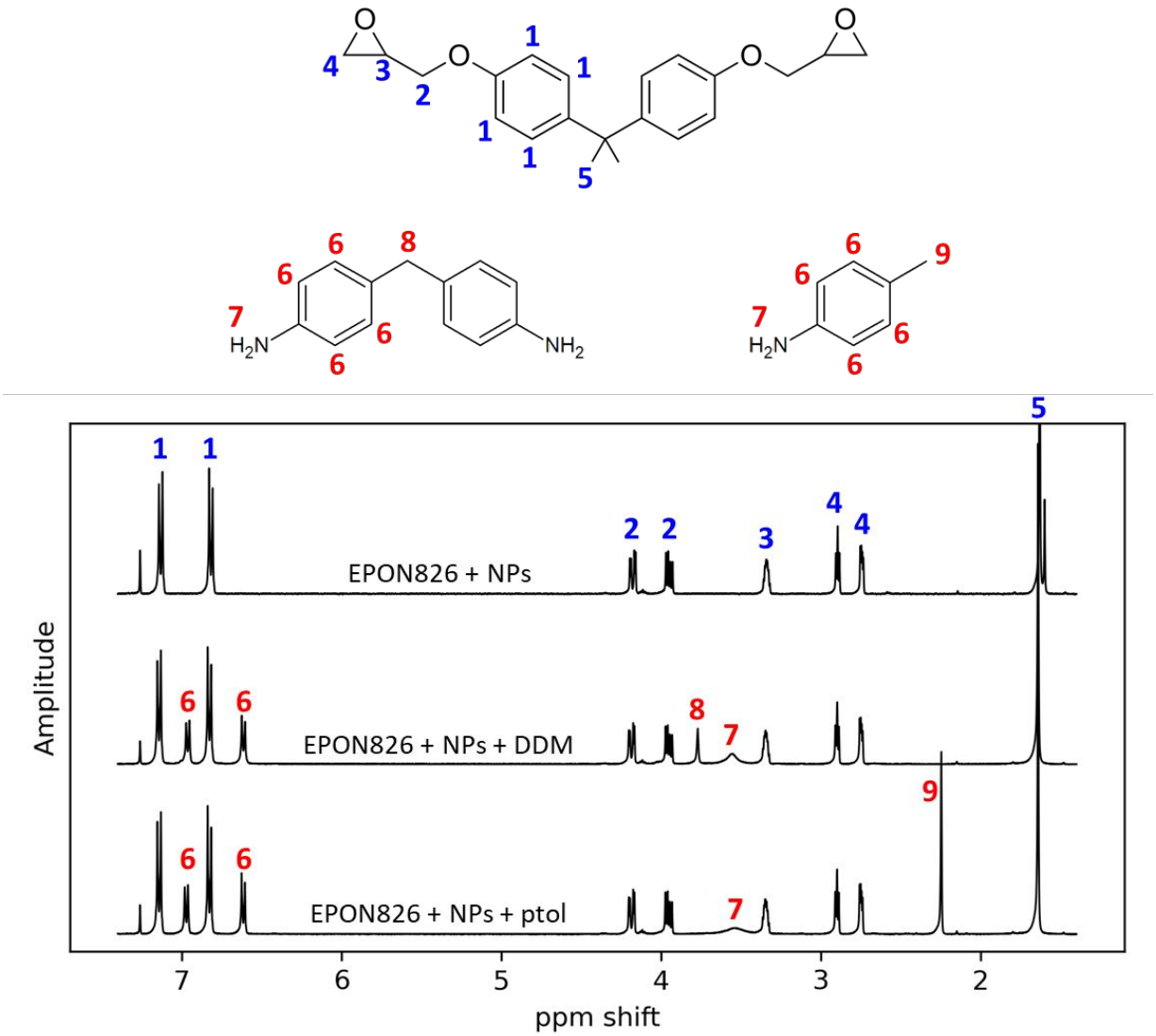

Figure S2. NMR spectroscopy of the EPON826-NP suspension before adding curing agent; after adding DDM; and after adding ptol. The data show that negligible reaction occurred during mixing.

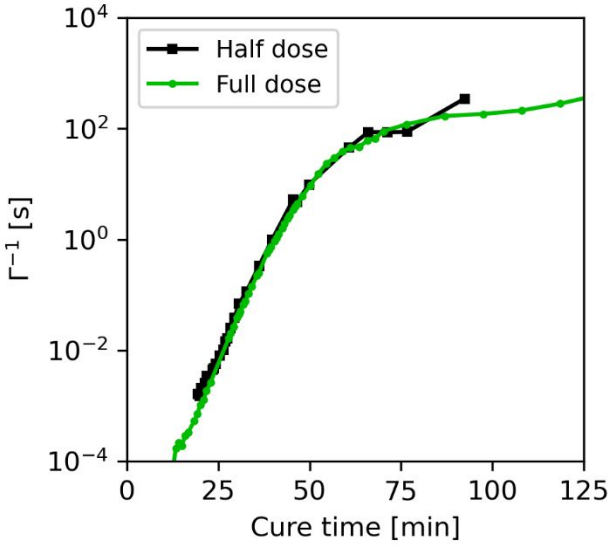

Figure S3. To test for beam damage, the *in situ* XPCS experiment was repeated for **ptol-90%**, while reducing the X-ray dose by a factor of two. (An attenuator was inserted to reduce incident beam intensity by a factor of five, while the number of speckle patterns in each series was increased by a factor of 2.5.) The relaxation time, Γ^{-1}, at q=0.01 $Å^{-1}$ versus cure time is plotted for both samples. Reducing the dose has virtually no effect on the relaxation rate, showing that the effect of the X-ray beam is minimal. The data with lower dose has substantially reduced signal-to-noise, leading to some scatter in Γ^{-1}.

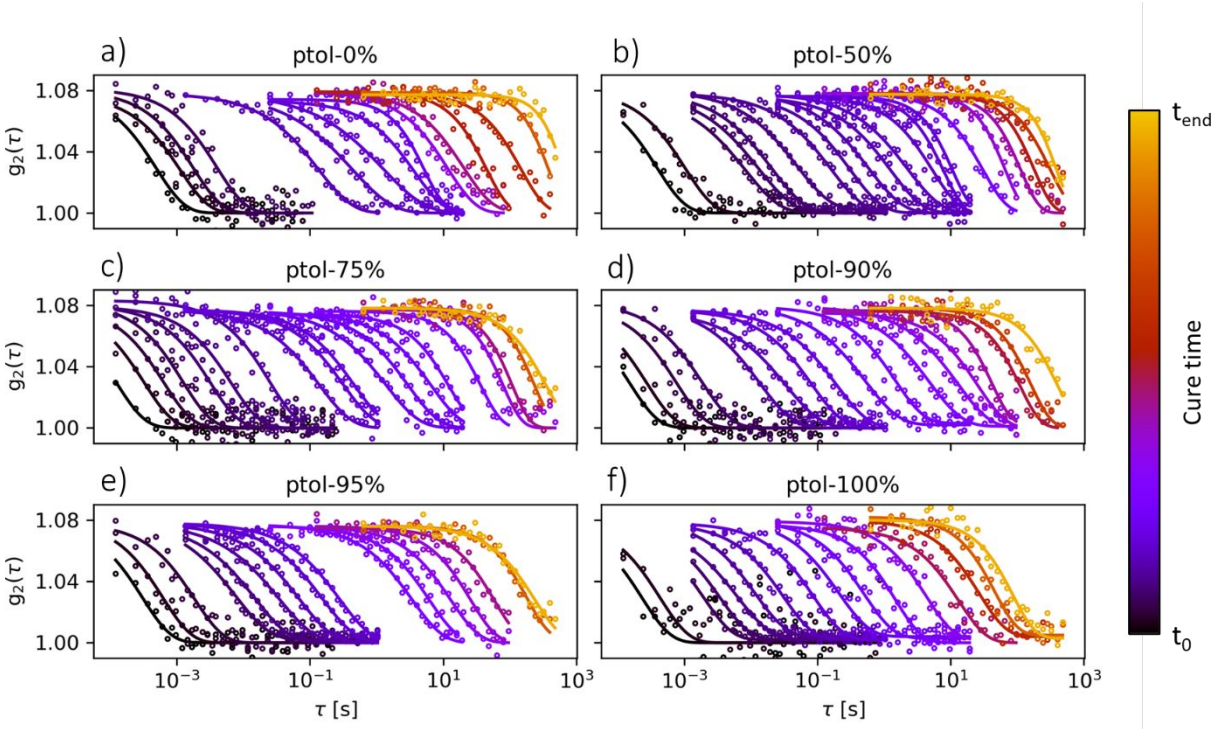

Figure S4. Selected g_2 curves (circles) and fits to Equation 1 (lines) for each of the six samples as labeled. All curves are at q=0.011 Å^{-1}. The color indicates cure time as depicted by the colorbar, and t_0 and t_{end} are different for each sample as follows:

Sample	**t_0 [min]**	**t_{end} [min]**
ptol-0%	9.1	63.7
ptol-50%	12.6	109.3
ptol-75%	11.4	114.2
ptol-90%	14.2	124.0
ptol-95%	17.7	126.3
ptol-100%	18.1	128.0

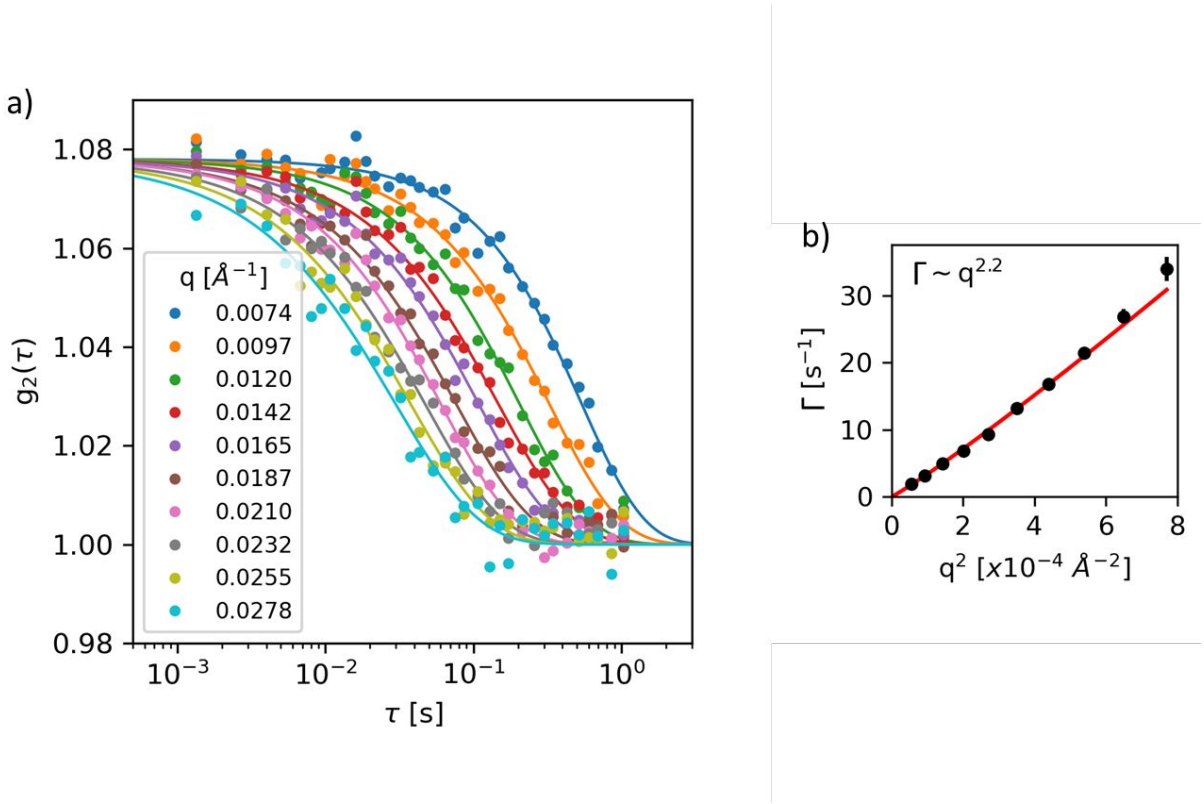

Figure S5. (a) Example of fits of g_2 curves to Equation 1. The legend indicates values of q in $Å^{-1}$. (b) Fit of relaxation rate Γ (obtained from fits in (a)) vs. q^2 to Equation 2. This dataset is **ptol-75%** at a cure time of 29 minutes. The frame rate for this dataset was 750 Hz.

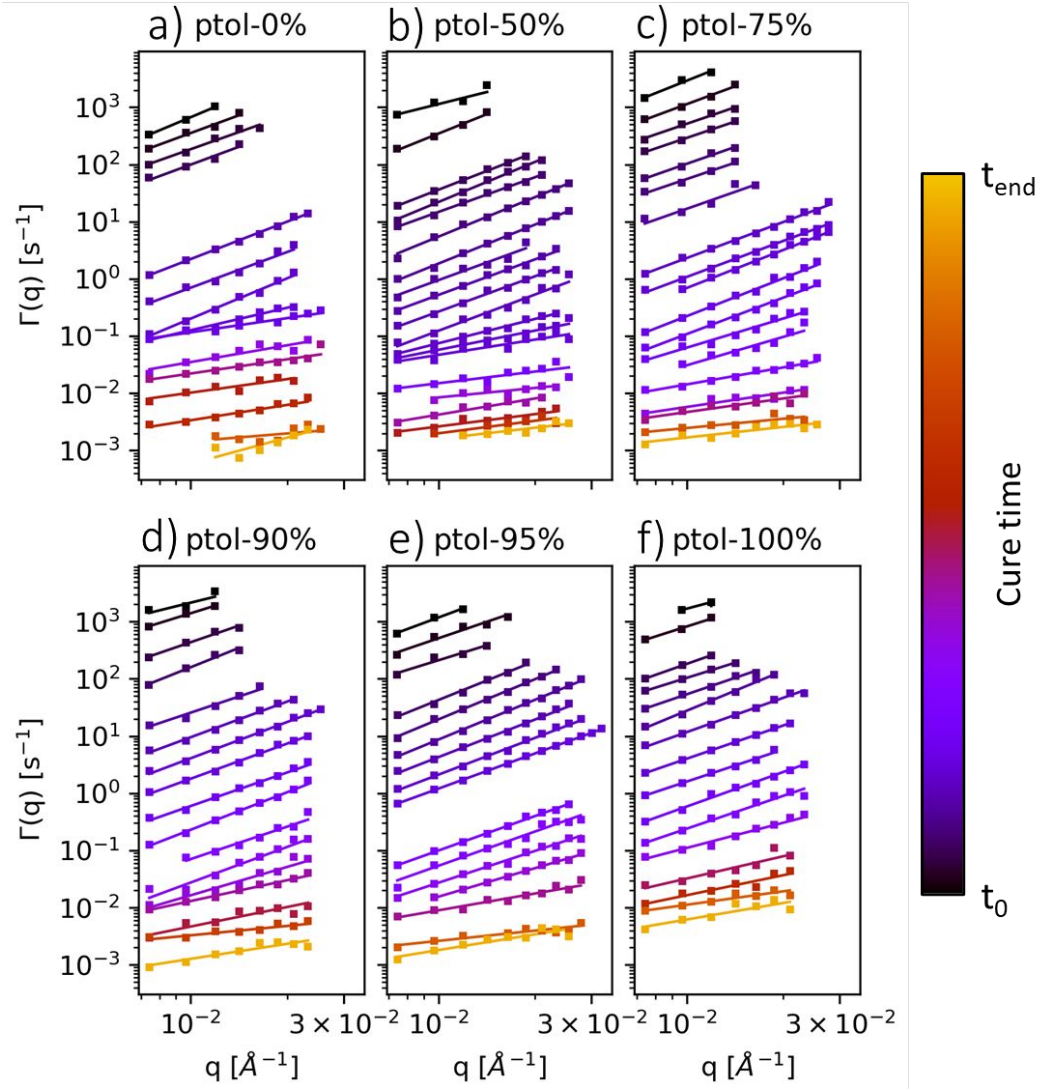

Figure S6. Selected Γ(q) data (squares), obtained from fits to g_2 to Equation 1 at several *q* values, for each of the six samples as labeled. The standard error of the fitting parameter Γ is smaller than the markers. Fits of Γ(q) to equation 2 are shown as lines. The color indicates cure time as depicted by the colorbar. The values of t_0 and t_{end} are different for each sample and are shown in the caption of Figure S4.

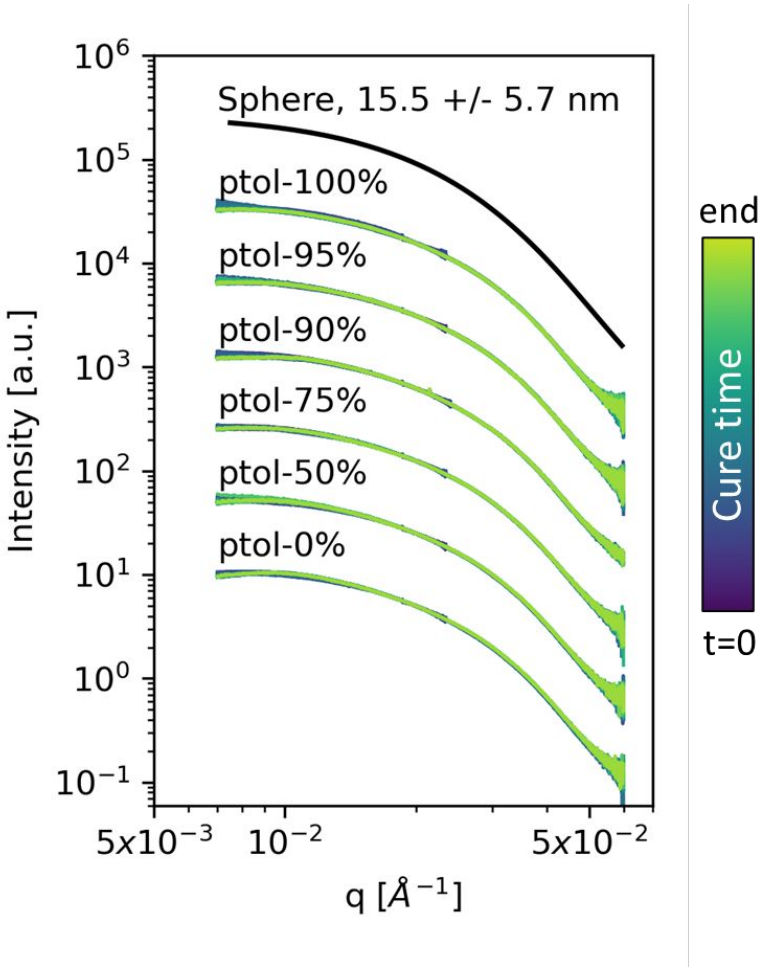

Figure S7. SAXS curves obtained during XPCS experiments for the six samples as labeled. Also plotted is the NP form factor from Figure S1 (black).

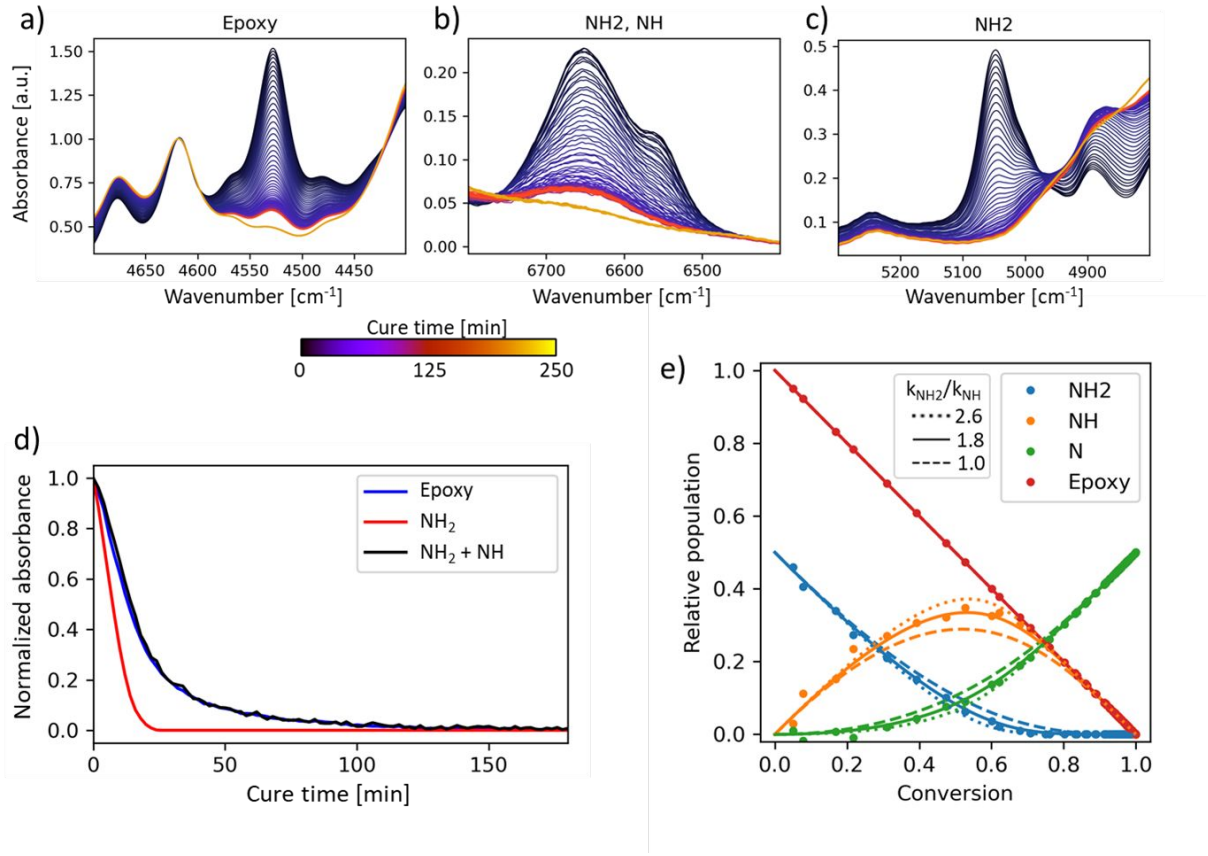

Figure S8. In situ FTIR during cure of **ptol-100%** at 110C. (a)-(c) Evolution of three spectral regions of interest during cure: (a) stretching and bending vibrations of the epoxide ring at 4530 cm^{-1}, (b) symmetric and antisymmetric stretching bands of both primary and secondary amines (6500-6700 cm^{-1}), and (c) stretching and bending band of primary amine only (5056 cm^{-1}).[2] (d) Absorbance of the three features in (a), (b), and (c) versus cure time, obtained by fitting with Gaussian functions, and normalized to the initial absorbance. The epoxy curve (blue) and the sum of primary and secondary amines curve (black) are indistinguishable, because their populations decline at the same rate. (e) Circles indicate the populations of the four species, calculated from (d), as a function of reaction conversion. The lines indicate theoretical curves based on a fixed reactivity ratio of primary to secondary amines, k_{NH2}/k_{NH}. The ratio of 1.8 agrees best with the experimental data.

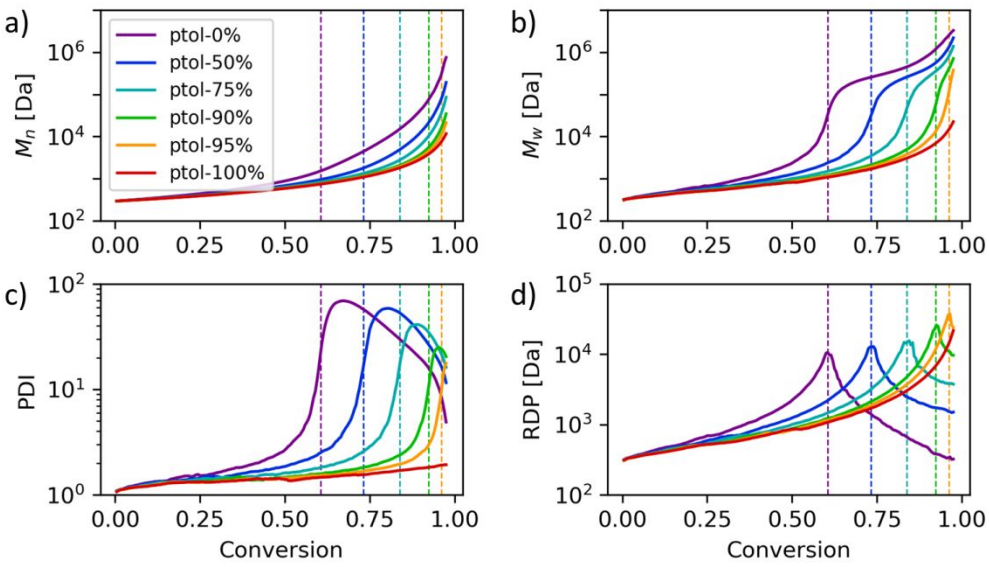

Figure S9. Monte Carlo simulation results for the six sample compositions. Plotted are (a) number-average molecular weight (M_n), (b) weight-average (M_w) molecular weight, (c) polydispersity index (PDI), and (d) reduced degree of polymerization (RDP), which is defined as the M_w excluding the largest molecule. The dashed lines are the gel points, obtained based on the peaks in RDP.[3] Each curve is the average of twenty simulations.

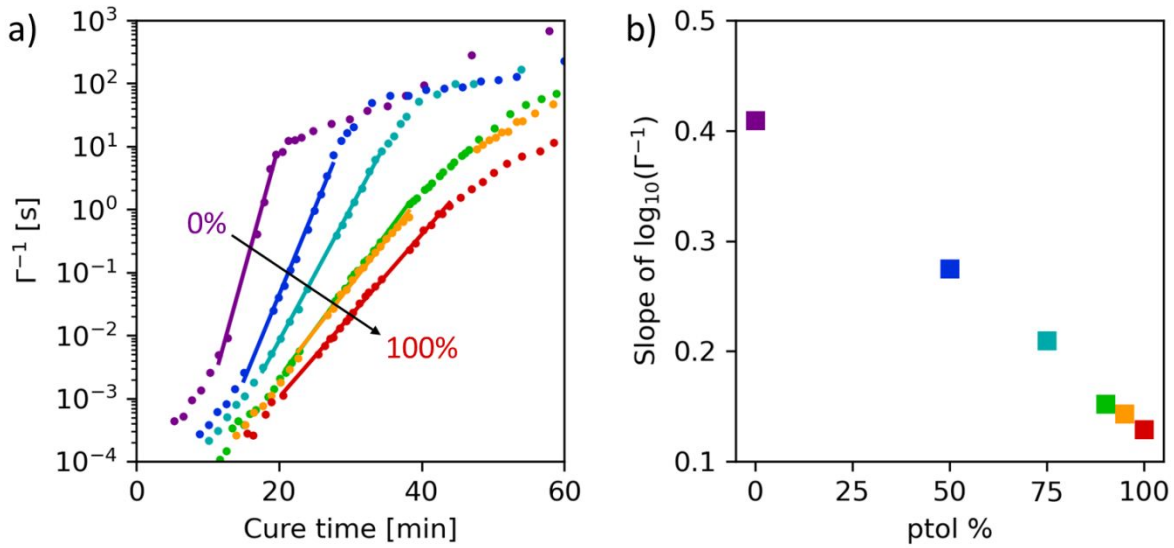

Figure S10. (a) For each sample, $\log_{10}(\Gamma^{-1})$ at q=0.011 Å^{-1} as a function of cure time is fit with a linear function at intermediate cure times (prior to the *p* transition). The data are shown as circles, and the fits are shown as solid lines. (b) The slope of $\log_{10}(\Gamma^{-1})$ based on the fit in (a) is shown for each sample.

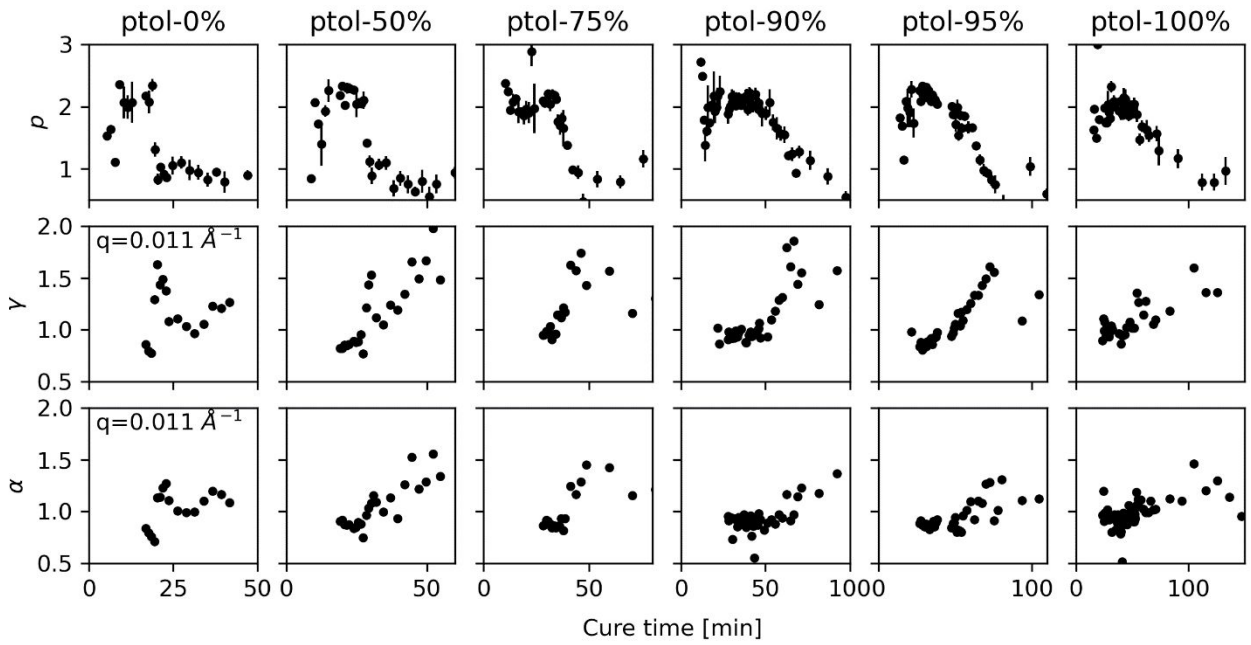

Figure S11. For the six samples (columns, as labeled), the following are plotted as a function of cure time: p, the scaling exponent of Γ with respect to q; γ, the compression exponent obtained from fitting g_2 to Equation 1; and α, as defined in Equation 3, obtained from the mean squared displacements. When p is slightly above 2, γ and α are approximately 1 (or slightly below), indicating a (nearly) diffusive relaxation. When p decreases to 1, γ and α increase to >1. γ and α are expected to be greater than 1 for a hyper-diffusive relaxation.

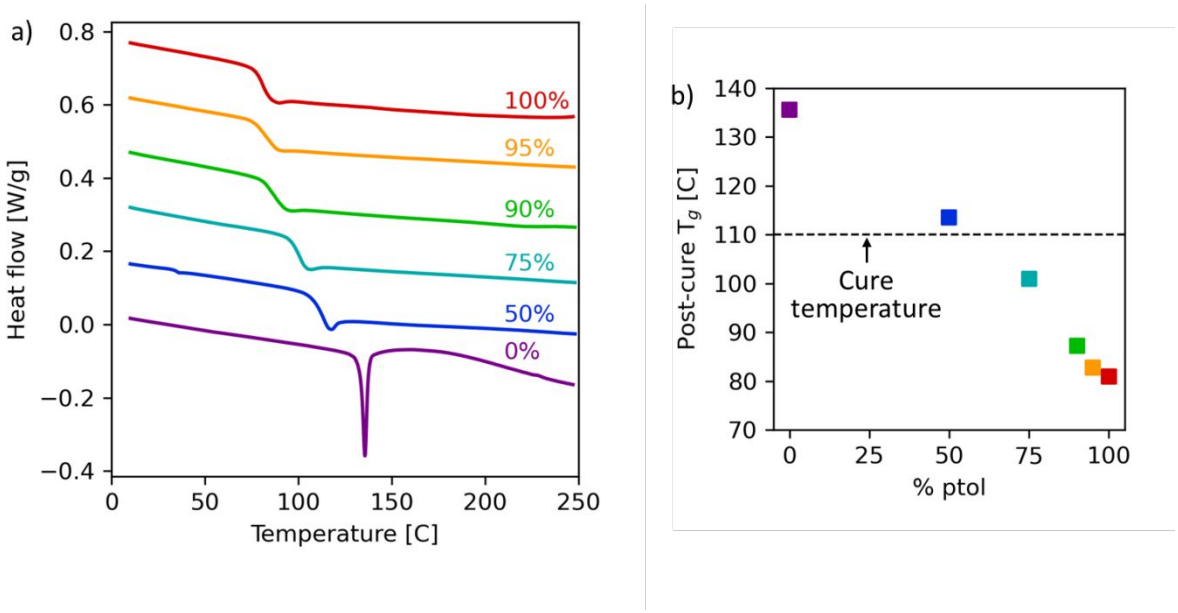

Figure S12. (a) Heating ramps after isothermal cure at 110°C, offset vertically for clarity. **ptol-0%** displays a large enthalpic relaxation at T_g, followed by a small exotherm that is the remainder of the reaction. The other samples show negligible exotherms above T_g, indicating that their curing reactions approached completion during the isothermal step. (b) Glass transition temperatures observed in the post-cure heating ramps.

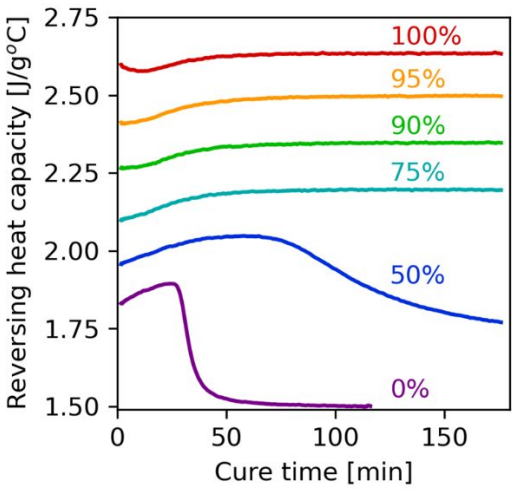

Figure S13. Reversing heat capacity as a function of cure time, via modulated DSC. A glass transition occurs in **ptol-0%** and **ptol-50%**, and manifests as a decline in heat capacity. Curves are offset vertically for clarity.

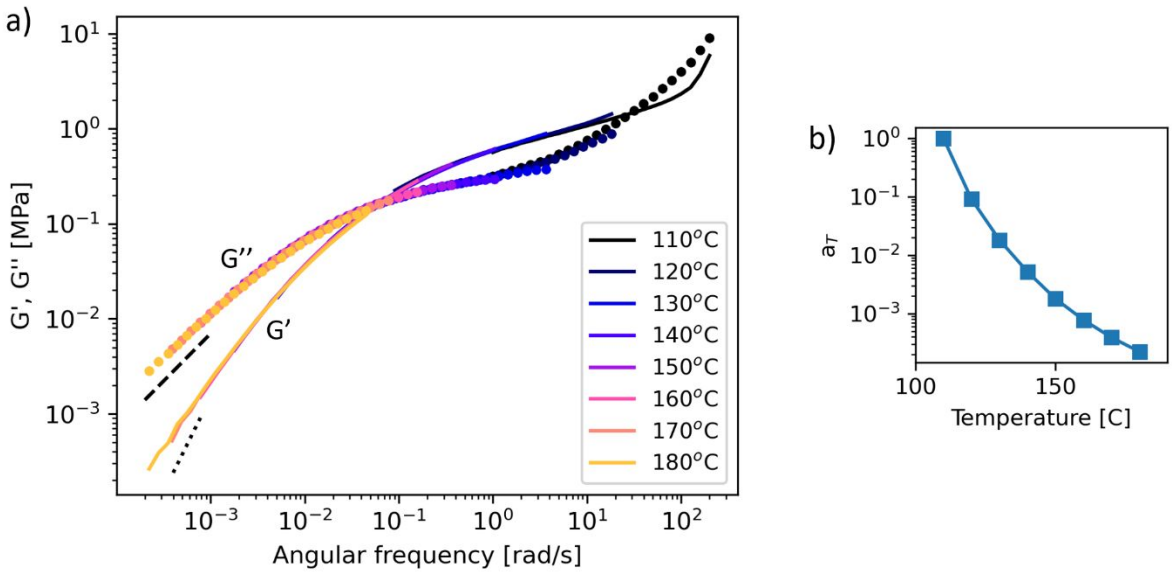

Figure S14. (a) Time-temperature superposition of bulk parallel plate rheology of **ptol-100%** after curing in a sealed vial at 110°C for 3 hours. The sample was hot-pressed at 120°C for 30 minutes, then loaded into the rheometer with 25 mm plates. Temperatures are indicated in the legend, and the reference temperature is 110°C. The low-frequency regime is consistent with terminal flow of a linear polymer (the dashed and dotted lines indicate slopes of 1 and 2, respectively), while the rubbery plateau at 10^{-1} – 10^{1} Hz indicates an entanglement network. (b) Shift factor as a function of inverse temperature, showing Arrhenius behavior at higher temperatures and Williams-Landel-Ferry-like behavior[4] at lower temperatures as T_g is approached.

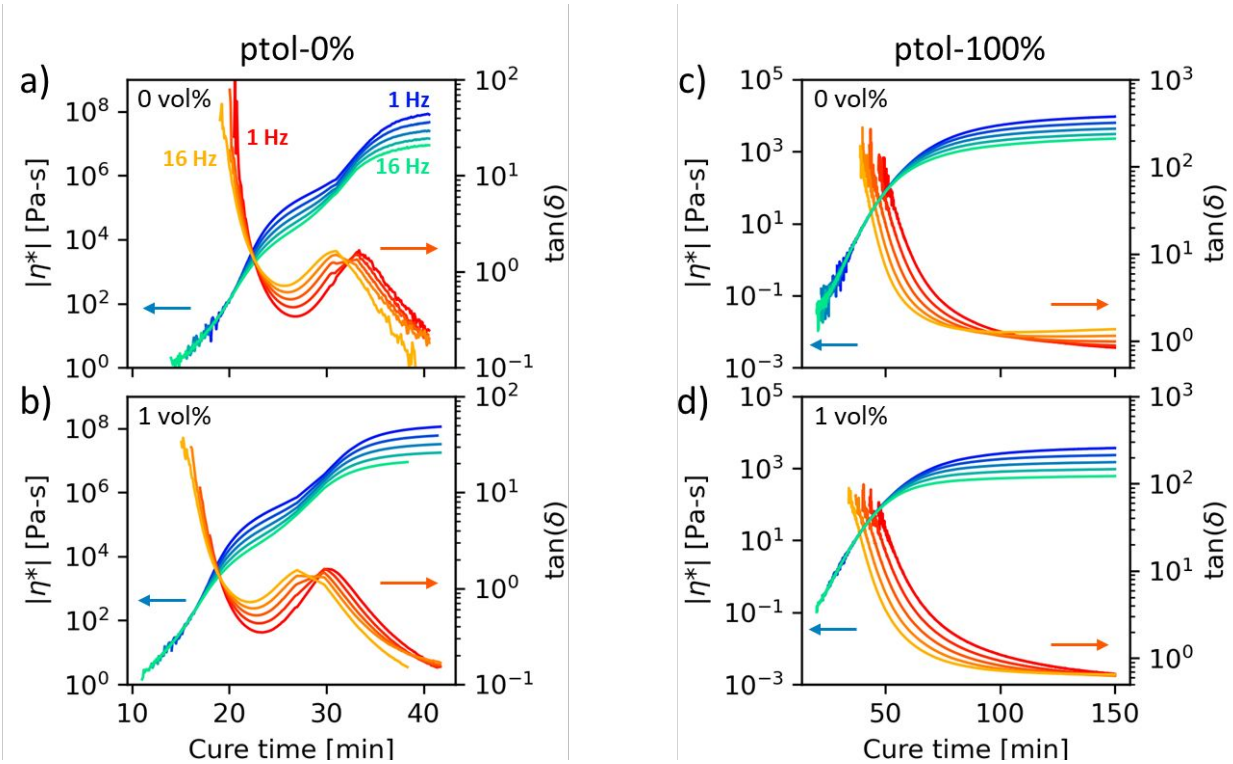

Figure S15. Shown is a comparison of rheological behavior with and without nanoparticles. Complex viscosity (blues) and tan(δ) (oranges) from bulk multiwave rheology are plotted during cure at 110C. (a) **ptol-0%** without NPs; (b) **ptol-0%** with 1 vol% NPs; (c) **ptol-100%** without NPs; (d) **ptol-100%** with 1 vol% NPs. Data are shown at five frequencies: 1, 2, 4, 8, and 16 Hz (lighter color = higher frequency).

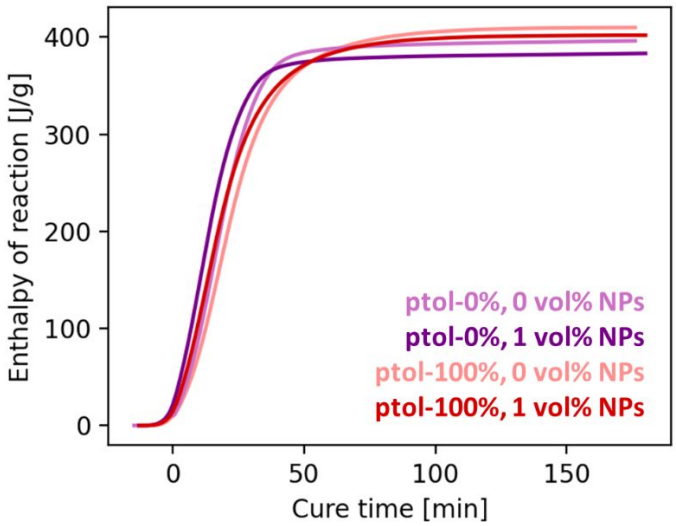

Figure S16. Effect of nanoparticles on cure kinetics of **ptol-0%** and **ptol-100%**. Plotted is the cumulative enthalpy of reaction versus cure time (DSC) for the unloaded resin and the 1 vol% loaded resin. For both samples, the addition of NPs increases the rate of reaction.

REFERENCES (SUPPORTING INFORMATION)

(1) Ilavsky, J.; Jemian, P. Irena: Tool Suite for Modeling and Analysis of Small-Angle Scattering. *J. Appl. Crystallogr.* **2009**, *42*, 347–353.

(2) Mijović, J.; Andjelić, S.; Kenny, J. M. In Situ Real-Time Monitoring of Epoxy/Amine Kinetics by Remote near Infrared Spectroscopy. *Polym. Adv. Technol.* **1996**, *7* (1), 1–16.

(3) Polanowski, P.; Jeszka, J. K.; Matyjaszewski, K. Modeling of Branching and Gelation in Living Copolymerization of Monomer and Divinyl Cross-Linker Using Dynamic Lattice Liquid Model (DLL) and Flory-Stockmayer Model. *Polymer* **2010**, *51* (25), 6084–6092.

(4) Williams, M. L.; Landel, R. F.; Ferry, J. D. The Temperature Dependence of Relaxation Mechanisms in Amorphous Polymers and Other Glass-Forming Liquids. *J. Am. Chem. Soc.* **1955**, *77* (14), 3701–3707.